Title
MOYER INTEGRALS FOR ESTIMATING SHIELDING OF HIGH-ENERGY ACCELERATORS

Authors
Routti, Jorma T.
Thomas, Ralph H.

Publication Date
1969-04-10

Submitted to Nuclear Instruments and Methods

UCRL-18862
Preprint

MOYER INTEGRALS FOR ESTIMATING SHIELDING OF HIGH-ENERGY ACCELERATORS

Jorma T. Routti and Ralph H. Thomas

April 10, 1969

AEC Contract No. W-7405-eng-48

LAWRENCE RADIATION LABORATORY
UNIVERSITY of CALIFORNIA BERKELEY

UCRL-18862
SUHP -69-1

MOYER INTEGRALS FOR ESTIMATING SHIELDING OF HIGH-ENERGY ACCELERATORS

Jorma T. Routti*

Lawrence Radiation Laboratory
University of California
Berkeley, California

and

Ralph H. Thomas*

Stanford University
Stanford, California

April 10, 1969

ABSTRACT

Integrals of the form $\int_0^{\pi} \exp(-\beta\theta) \exp(-\ell \operatorname{cosec}\theta) d\theta$ often arise in the calculation of shielding for high energy accelerators. These integrals have been named "Moyer Integrals" and numerically evaluated in the region of practical interest. Examples are given to show how these integrals may be used to estimate shielding in practical situations.

1. Introduction

In 1961 Moyer[1,2] described a semi-empirical method for evaluating shielding for the Bevatron—the 6-GeV proton synchrotron of the Lawrence Radiation Laboratory. The value of this technique for high energy accelerator shielding calculations is indicated by good agreement between calculated and measured radiation levels outside the Bevatron shielding[3]. Smith[4] has given a detailed discussion of the experimental evaluation of the Bevatron shielding performance.

DeStaebler[5] generalized this semi-empirical method and used it in shielding estimation for the 20-GeV electron linear accelerator at Stanford. It was DeStaebler who first used the designation "Method of Moyer" which has been generally adopted. To quote DeStaebler— "Our name for this method and our description of it have not been sanctioned by Professor Moyer, and we apologize if we have said anything which embarrasses him."

More recently[6] Moyer's Method was used to predict shielding for a 200-GeV proton synchrotron. Results in good agreement with alternative calculations were obtained despite the severe limitations of input data.

As part of a continuing program of high-energy radiation studies at CERN, the Lawrence Radiation Laboratory, and the Rutherford High Energy Laboratory, an extensive shielding experiment has been made at the CERN 25-GeV proton synchrotron. Preliminary data obtained from these measurements have been published[7-9], and an extensive report covers the results in detail[10]. This experiment has given strong experimental justifications for the semi-empirical method of shielding calculations originally due to Moyer.

2. Brief Description of the Moyer Method of Calculating Shielding

Detailed descriptions of the Method of Moyer have been published in the literature[1,2,3,5,6,10]. For the physical justification of the method the reader is referred to these papers. However, for the sake of clarity a brief description is given here.

A proton accelerator may be considered, for the purpose of calculating shielding, as a source of neutrons. In the high-energy strong-focusing proton synchrotrons it is sufficiently accurate to ignore the radial curvature of the accelerator. Figure 1 shows a typical two-dimensional representation of the accelerator as a line source of neutrons of variable intensity.

The neutron flux, ϕ, at a point outside the shield is expressed as

$$\phi = \int_{-\infty}^{\infty} \int_{E_{min}}^{E_{max}} S(z)\, f(E,\theta)\, r^{-2} \exp\left(- \frac{d \operatorname{cosec} \theta}{\lambda(E)}\right) B(E,\theta)\, dE\, dz \qquad (1)$$

where a, d, r, and θ are explained by fig. 1,

- $S(z)\,dz$ is the number of neutrons emitted in unit time by the line element between z and $z+dz$,
- $f(E,\theta)$ is the distribution of the neutrons emitted as a function of the energy and the angle, per steradian,
- $\lambda(E)$ is the attenuation length of neutrons of energy E in the shield, and
- $B(E,\theta)$ is the buildup factor as a function of the energy and the geometry.

The integration is carried over the appropriate limits of z and E.

Experimental data given by Patterson[11]) indicate that the attenuation length of neutrons increases with increasing energy up to about 150 MeV and remains approximately constant beyond that. After a few mean free paths of shielding the nuclear cascade generated by the slowing down of the high energy neutrons through elastic and inelastic scattering gives rise to the formation of an equilibrium spectrum whose attenuation is determined by the fast component above 150 MeV. This justifies the essential simplification made by Moyer in his calculational method to consider only neutrons above 150 MeV. We can then write

$$\lambda(E) \approx \lambda,$$
$$\int_{E_{min}}^{E_{max}} f(E,\theta)\,dE \approx g(\theta)\,, \qquad (2)$$
$$B(E,\theta) \approx 1,$$

where $g(\theta)$ is the angular distribution of neutrons with more than 150 MeV energy. Hence the high energy flux is expressed as

$$\phi(E_n > 150\text{ MeV}) = \int_{-\infty}^{\infty} S(z)\, g(\theta)\, r^{-2} \exp\left(-\frac{d \operatorname{cosec}\theta}{\lambda}\right) dz. \qquad (3)$$

If we consider the case of constant beam loss, that is $S(z) = S$, and change the variable z to θ in the above equation, and use the relations

$$r = (a + d) \operatorname{cosec}\theta,$$
$$dz = (a + d) \operatorname{cosec}^2\theta\, d\theta, \qquad (4)$$

we obtain for the high-energy flux above a given threshold energy, E_t, the expression

$$\phi(E_n > E_t) = \frac{S}{a+d} \int_0^{\pi} g(\theta) \exp\left(-\frac{d \operatorname{cosec}\theta}{\lambda}\right) d\theta \qquad (5)$$

Here $g(\theta)$ is an appropriate angular distribution for source neutrons of energy greater than E_t, per steradian.

3. Angular Distribution of Neutrons

Measurements of the angular distribution of neutrons from a thin beryllium target were made by using threshold detectors as a part of the CERN-LRL-RHEL shielding study[10)]. Accurate measurements around targets inside the main accelerator vacuum chamber are difficult because of interference from adjacent beam losses. The results, however, when corrected for this interference are supported by similar results from measurements made by Charalambus et al.[12)].

The results from activation detectors with thresholds of 20 and 600 MeV are in fair agreement with the angular distribution predicted from the production formula due to Ranft[13)], based on the measurements of the pion and proton yields at small angles from thin targets. Figures 2 and 3 show the comparison of the CERN-LRL-RHEL measurements of the angular distributions made by using $^{12}C \rightarrow {}^{11}C$ (20 MeV threshold) and $Hg \rightarrow {}^{149}Tb$ (600 MeV threshold) activation detectors with values calculated from the Ranft formula[14)].

The combined effect of the angular distribution of the neutrons produced and the attenuation geometry means that the transverse shield thickness for a high energy accelerator is largely determined by the number of neutrons emitted around 90 deg to the incident proton beam. In the region of $\theta \approx 90$ deg the angular distribution is well approximated by the simple exponential function

$$g(\theta) \approx \alpha \exp(-\beta\theta). \qquad (6)$$

The slope of the curve increases with the threshold energy, and a value close to 4 is obtained for β from the calculated curves, as shown in fig. 4. Figure 5 gives values of β calculated from Ranft formulae for different threshold energies.

4. Moyer Integrals

Substituting the exponential approximation for $g(\theta)$ in Eq. (5) yields

$$\phi(E_n > E_t) = \frac{\alpha S}{(a+d)} \int_0^{\pi} \exp(-\beta\,\theta)\, \exp\left(-\frac{d \operatorname{cosec}\theta}{\lambda}\right) d\theta \,. \tag{7}$$

We define the Moyer Integral

$$M(\beta, \ell) = \int_0^{\pi} \exp(-\beta\,\theta)\, \exp(-\ell \operatorname{cosec}\theta)\, d\theta, \tag{8}$$

which is a function of the angular distribution coefficient β and the number of mean free paths in the shield ℓ, $\ell = d/\lambda$. The solution of shielding problems is often facilitated by the use of these integrals.

We have evaluated the Moyer Integrals in the region of physical interest for the solution of practical shielding problems. Because of the interest in high energy accelerators of energies up to 500 GeV these calculations have been extended for values of ℓ up to 40 and β up to 15. An iterative Simpson's-rule algorithm was employed to compute the integrals with an accuracy of 0.1%. The tabulated values of $M(\beta, \ell)$ are given in table 1.

The general form of the Moyer Integrals is shown in fig. 6 and on an expanded scale in fig. 7. It is seen that with an increasingly forward-peaked angular distribution--that is, increasing β--the transmission of the shield is reduced. At larger depths the curves may be approximated, for most practical purposes, by simple exponentials.

This approximation becomes better the smaller the value of β or the larger the value of ℓ. At very large depths the effective slope of the Moyer Integral corresponds to the mean free path in the shield, but at values of practical interest--that is, 10 to 15 mean free paths--the effective slope is somewhat steeper. For $\beta \approx 4$, corresponding to 150 MeV threshold energy, the slope is about 7% steeper.

5. Use of Moyer Integrals to Estimate Shielding Thickness

We have shown that the flux of high energy neutrons at the surface of the shield can be expressed as

$$\phi(E_n > E_t) = \frac{\alpha S}{a+d} M(\beta, \ell) . \tag{9}$$

The term S is proportional to the incident beam loss, B, and also to the energy, E_0, above 10 GeV[14]. It follows from the properties of the nuclear cascade as briefly described in section 2 that the dose-equivalent rate, D, is proportional to $\phi(E_n > 150 \text{ MeV})$, and is then expressed as

$$D = \text{constant} \times \frac{BE_0}{a+d} M(\beta, \ell) \tag{10}$$

or

$$D = C \frac{L}{a+d} M(\beta, \ell) , \tag{11}$$

where $L = BE_0$ is the energy loss from the accelerator vacuum chamber.

The value of the normalizing constant C appearing in eq. (11) may be obtained from the data of the CERN-LRL-RHEL experiment. Gilbert et al.[10] have shown that the average energy loss in the CERN proton synchrotron, of radius 100 meters and operating with 2×10^{11} protons/sec at 25.5 GeV, is under normal conditions 8.1×10^7 GeV/cm. sec. During the experiment the use of a thin target and a beam clipper, however, reduced this in quiet areas to an effective value of 1.8×10^7 GeV/cm. sec[10].

The CPS earth shield is 685 g/cm^2 thick or approximately 3.2 m of earth of density 2.16 g/cm^3. The attenuation length of high energy neutrons in this earth is 53.9 cm or 116.5 g/cm^2. In the CPS machine the magnet adds to the earth shield about 400 g/cm^2. The internal accelerator tunnel is of 2.8 m radius. The dose-equivalent rate at the earth shield surface corresponding to this beam loss was 0.8 mrem/h. By substituting the values $D = 0.8$ mrem/h, $L = 1.8\times10^7$ GeV/cm. sec, $a = 2.8$ m, $d = 3.2$ m, $\beta = 4$ corresponding to 150 MeV threshold, $\ell = (685+400)/116.5 = 9.3$, and $M(4, 9.3) = 2.6\times10^{-7}$ into eq. (11), we obtain a very convenient value of normalizing constant, $C = 1.0$. If the magnet is assumed to be always 400 g/cm^2 thick, then for evaluating the earth shield alone the constant would be 0.022, with the above units for the other quantities.

The dose-equivalent rate can thus be expressed as

$$D[\text{mrem/h}] = \frac{L[\text{GeV/cm. sec}]}{(a+d)\,[\text{m}]}\, M(4,\ell)\,. \tag{12}$$

The shielding calculations of large proton synchrotrons may be carried out with great facility by using this simple relation and the tabulated values of the Moyer Integrals. As an example we consider the determination of shield thickness for the proposed 200-GeV machine by using the values given in the LRL design study[6]. The average energy loss with 2×10^{12} protons/sec beam in the ring of 693 m radius is 9.2×10^8 GeV/cm. sec. We assume the effective magnet thickness to be 280 g/cm^2, and again take $a = 2.8$ m, $\beta = 4$, and $\lambda = 53.9$ cm, and determine d for the given dose rate, 1.25 mrem/h. A simple interpolation between the trial values $D_{d=5\ m} = 2.1$ mrem/h, $D_{d=6\ m} = 0.3$ mrem/h, and $D_{d=5.5\ m} = 0.8$ mrem/h yields the desired shield thickness of 5.3 m of earth shield or 1430 g/cm^2 total shield.

We have made similar calculations of shield thicknesses for the improved CERN proton synchrotron and the 200-GeV and 300-GeV machines under design at present. Assumptions as to the beam losses were taken from the original documents[6, 15]. The accelerator tunnel is taken to be of 2.8 m radius in each case. Table 2 lists the results obtained with Moyer integrals and in the CERN-LRL-RHEL study[10]. The excellent agreement with estimates made by using a more sophisticated technique, described by Gilbert et al.[10], is obvious.

These results are also summarized in fig. 8. The results from the Moyer Integral method can be well approximated by a straight line drawn on the graph. For the case considered--that is, $\beta = 4$, $\lambda = 53.9$ cm (or 116.5 g cm^{-2}), a = 2.8 m--we then obtain for the required total shielding thickness, t, as a function of L/D, the simple expression

$$t\,[\mathrm{g/cm^2}] = 230 \log_{10}\left(\frac{L\,[\mathrm{GeV/cm\cdot sec}]}{D\,[\mathrm{mrem/h}]}\right) - 610. \qquad (13)$$

Above the internal targets the use of this simple formula is not very precise. Typically the value of L/D above the targets is some two orders of magnitude higher than in the regions of low beam loss. Such an assumption with the Moyer Integrals leads to a conservative estimate. For precise shield configurations detailed beam-loss distribution should be used.

In summary, the use of the Moyer Integrals allows rapid and accurate estimates of the high-energy neutron flux above different threshold energies as well as the dose-equivalent rate to be found at the surface of proton accelerator shields operating in the energy region 5 to 500 GeV.

The precision for the flux and dose rate estimates in regions of uniform beam loss is likely to be better than a factor of two, and even in target regions the dose-rate estimates are fairly reliable.

ACKNOWLEDGMENTS

The authors are indebted to their colleagues at their laboratories and in particular to the members of the CERN-LRL-Rutherford Laboratory Shielding Experiment, who provided much of the available experimental data. They wish to thank H. Wade Patterson and Alan R. Smith for their cooperation, and last but not least, Professor Burton J. Moyer for his original idea.

REFERENCES

1. B. J. Moyer, Evaluation of shielding required for the improved Bevatron, UCRL-9769 (1961).

2. B. J. Moyer, Method of calculation of the shielding enclosure for the Berkeley Bevatron in First International Conference on Shielding Around High Energy Accelerators (Presses Universitaires de France, Paris, 1962), P. 65.

3. R. H. Thomas, Shielding of the Bevatron - to be published in Engineering Compendium on Radiation, Vol. 2, IAEA (Springer-Verlag, Berlin, 1969).

4. A. R. Smith, Some experimental shielding studies at the 6.2-GeV Berkeley Bevatron, in Proceedings of the USAEC First Symposium on Accelerator Radiation Dosimetry and Experience, CONF-651109 (1965).

5. H. DeStaebler, Transverse Radiation Shielding for the Stanford Two-Mile Accelerator, SLAC 9, Stanford University, California (1962).

6. 200 BeV Accelerator Design Study - UCRL-16000, June 1965. Chap. XII.

7. W. S. Gilbert, Radiation problems with high energy proton accelerators, UCRL-1741, Feb. 1967; paper read at Particle Accelerator Conference, March 1-3, 1967, Washington, D. C.

8. R. D. Fortune, W. S. Gilbert, and R. H. Thomas, Shielding experiment at the CERN PS, UCRL internal document UCID-10199, April 1967.

9. W. S. Gilbert, Beam loss and shielding relevant to high energy proton synchrotrons, in Proceedings of the 6th International Conference

on High Energy Accelerators, 1967, CEAL 2000 (also published as UCRL-17797).

10. W. S. Gilbert, et al., 1966 CERN-LRL-RHEL shielding experiment at the CERN proton synchrotron, UCRL-17941, Sept. 1968.

11. H. W. Patterson, The effect of shielding on radiation produced by the 730-MeV synchrocyclotron and the 6.3-GeV proton synchrotron at the Lawrence Radiation Laboratory, in The First International Conference on Accelerators, Saclay, 1962.

12. S. Charalambus, et al., CERN DI/HP/67, March 14, 1967.

13. J. Ranft, Improved Monte-Carlo Calculation of the Nuclear-Meson Cascade in Shielding Material. I. Description of the Method of Calculation, Nucl. Instr. and Meth. 48 (1967) 133.

14. J. T. Routti, R. H. Thomas, Angular Distribution of Secondary Neutrons and Protons from High-Energy Interactions (in preparation).

15. Report on the design study of a 300-GeV proton synchrotron by CERN Study Group on New Accelerators, CERN/563, Nov. 1964, (2 vols.).

Table I. Tabulated values of Moyer Integrals $M(\beta, \ell) = \int_0^{\pi} \exp(-\beta\theta)\exp(-\ell \operatorname{cosec}\theta)\,d\theta$

ℓ \ β	0	1	1.6	2	3	4	5	6	7	8	9	10
0.	3.14E+00	9.56E-01	6.20E-01	4.98E-01	3.32E-01	2.49E-01	1.99E-01	1.66E-01	1.42E-01	1.24E-01	1.10E-01	9.90E-02
.25	1.88E+00	5.11E-01	2.90E-01	2.12E-01	1.13E-01	6.85E-02	4.53E-02	3.17E-02	2.30E-02	1.73E-02	1.32E-02	1.04E-02
.50	1.29E+00	3.34E-01	1.80E-01	1.26E-01	6.02E-02	3.32E-02	2.01E-02	1.29E-02	8.69E-03	6.06E-03	4.34E-03	3.18E-03
1.00	6.57E-01	1.62E-01	8.17E-02	5.44E-02	2.27E-02	1.10E-02	5.87E-03	3.36E-03	2.03E-03	1.28E-03	8.34E-04	5.58E-04
1.50	3.52E-01	8.46E-02	4.09E-02	2.64E-02	1.00E-02	4.42E-03	2.16E-03	1.14E-03	6.34E-04	3.70E-04	2.24E-04	1.40E-04
2.00	1.94E-01	4.57E-02	2.15E-02	1.35E-02	4.81E-03	1.97E-03	8.96E-04	4.40E-04	2.30E-04	1.26E-04	7.20E-05	4.25E-05
3.00	6.17E-02	1.41E-02	6.39E-03	3.90E-03	1.26E-03	4.64E-04	1.89E-04	8.33E-05	3.92E-05	1.94E-05	1.01E-05	5.41E-06
4.00	2.03E-02	4.57E-03	2.02E-03	1.20E-03	3.64E-04	1.24E-04	4.65E-05	1.89E-05	8.18E-06	3.75E-06	1.80E-06	8.96E-07
5.00	6.82E-03	1.52E-03	6.58E-04	3.87E-04	1.11E-04	3.58E-05	1.26E-05	4.78E-06	1.94E-06	8.30E-07	3.73E-07	1.75E-07
6.00	2.32E-03	5.13E-04	2.20E-04	1.28E-04	3.54E-05	1.08E-05	3.62E-06	1.30E-06	4.99E-07	2.02E-07	8.60E-08	3.81E-08
7.00	8.00E-04	1.76E-04	7.43E-05	4.28E-05	1.15E-05	3.40E-06	1.09E-06	3.74E-07	1.37E-07	5.28E-08	2.14E-08	9.03E-09
8.00	2.78E-04	6.06E-05	2.55E-05	1.45E-05	3.83E-06	1.09E-06	3.38E-07	1.12E-07	3.91E-08	1.45E-08	5.62E-09	2.28E-09
9.00	9.70E-05	2.11E-05	8.79E-06	4.99E-06	1.29E-06	3.59E-07	1.07E-07	3.43E-08	1.16E-08	4.14E-09	1.55E-09	6.04E-10
10.00	3.40E-05	7.37E-06	3.06E-06	1.73E-06	4.38E-07	1.19E-07	3.48E-08	1.08E-08	3.54E-09	1.22E-09	4.42E-10	1.67E-10
12.00	4.24E-06	9.13E-07	3.75E-07	2.11E-07	5.19E-08	1.37E-08	3.81E-09	1.13E-09	3.51E-10	1.15E-10	3.91E-11	1.39E-11
14.00	5.35E-07	1.15E-07	4.68E-08	2.61E-08	6.31E-09	1.61E-09	4.36E-10	1.24E-10	3.70E-11	1.16E-11	3.76E-12	1.27E-12
16.00	6.80E-08	1.45E-08	5.91E-09	3.28E-09	7.79E-10	1.95E-10	5.13E-11	1.42E-11	4.08E-12	1.23E-12	3.84E-13	1.25E-13
18.00	8.71E-09	1.86E-09	7.51E-10	4.15E-10	9.74E-11	2.40E-11	6.17E-12	1.66E-12	4.65E-13	1.36E-13	4.10E-14	1.29E-14
20.00	1.12E-09	2.39E-10	9.62E-11	5.30E-11	1.23E-11	2.98E-12	7.54E-13	1.98E-13	5.43E-14	1.54E-14	4.53E-15	1.38E-15
22.00	1.45E-10	3.08E-11	1.24E-11	6.81E-12	1.57E-12	3.75E-13	9.33E-14	2.41E-14	6.46E-15	1.79E-15	5.15E-16	1.53E-16
24.00	1.88E-11	3.99E-12	1.60E-12	8.78E-13	2.01E-13	4.75E-14	1.17E-14	2.97E-15	7.82E-16	2.13E-16	5.97E-17	1.73E-17
25.00	6.80E-12	1.44E-12	5.77E-13	3.16E-13	7.19E-14	1.70E-14	4.14E-15	1.05E-15	2.73E-16	7.37E-17	2.05E-17	5.87E-18
26.00	2.45E-12	5.19E-13	2.08E-13	1.14E-13	2.58E-14	6.06E-15	1.47E-15	3.70E-16	9.58E-17	2.56E-17	7.06E-18	2.00E-18
28.00	3.21E-13	6.78E-14	2.71E-14	1.48E-14	3.34E-15	7.78E-16	1.87E-16	4.64E-17	1.19E-17	3.12E-18	8.46E-19	2.36E-19
30.00	4.20E-14	8.86E-15	3.54E-15	1.93E-15	4.33E-16	1.00E-16	2.39E-17	5.86E-18	1.48E-18	3.85E-19	1.03E-19	2.91E-20
32.00	5.51E-15	1.16E-15	4.63E-16	2.52E-16	5.64E-17	1.30E-17	3.07E-18	7.45E-19	1.86E-19	4.78E-20	1.26E-20	3.40E-21
34.00	7.24E-16	1.53E-16	6.07E-17	3.30E-17	7.36E-18	1.68E-18	3.95E-19	9.53E-20	2.36E-20	5.98E-21	1.56E-21	4.15E-22
35.00	2.63E-16	5.53E-17	2.20E-17	1.20E-17	2.66E-18	6.07E-19	1.42E-19	3.41E-20	8.41E-21	2.12E-21	5.40E-22	1.46E-22
36.00	9.53E-17	2.01E-17	7.98E-18	4.34E-18	9.62E-19	2.19E-19	5.11E-20	1.22E-20	3.00E-21	7.54E-22	1.94E-22	5.11E-23
38.00	1.26E-17	2.64E-18	1.05E-18	5.70E-19	1.26E-19	2.86E-20	6.63E-21	1.58E-21	3.84E-22	9.55E-23	2.44E-23	6.35E-24
40.00	1.66E-18	3.49E-19	1.38E-19	7.51E-20	1.66E-20	3.74E-21	8.63E-22	2.04E-22	4.93E-23	1.22E-23	3.07E-24	7.93E-25

ℓ \ β	11	12	13	14	15	16	18	20	22	24	27	30
0.	8.99E-02	8.23E-02	7.59E-02	7.04E-02	6.57E-02	6.15E-02	5.46E-02	4.90E-02	4.45E-02	4.07E-02	3.61E-02	3.23E-02
.25	8.24E-03	6.64E-03	5.41E-03	4.45E-03	3.70E-03	3.10E-03	2.22E-03	1.62E-03	1.21E-03	9.19E-04	6.23E-04	4.33E-04
.50	2.38E-03	1.81E-03	1.39E-03	1.08E-03	8.54E-04	6.79E-04	4.40E-04	2.94E-04	2.00E-04	1.40E-04	8.38E-05	5.20E-05
1.00	3.82E-04	2.67E-04	1.90E-04	1.37E-04	9.99E-05	7.39E-05	4.17E-05	2.44E-05	1.47E-05	9.05E-06	4.58E-06	2.41E-06
1.50	8.98E-05	5.89E-05	3.93E-05	2.67E-05	1.85E-05	1.29E-05	6.55E-06	3.46E-06	1.89E-06	1.07E-06	4.73E-07	2.20E-07
2.00	2.58E-05	1.60E-05	1.02E-05	6.59E-06	4.34E-06	2.90E-06	1.34E-06	6.53E-07	3.30E-07	1.72E-07	6.83E-08	2.86E-08
3.00	3.00E-06	1.71E-06	1.00E-06	5.97E-07	3.63E-07	2.25E-07	9.00E-08	3.80E-08	1.68E-08	7.71E-09	2.55E-09	9.98E-10
4.00	4.62E-07	2.45E-07	1.34E-07	7.48E-08	4.26E-08	2.48E-08	8.79E-09	3.31E-09	1.31E-09	5.39E-10	1.50E-10	4.67E-11
5.00	8.47E-08	4.24E-08	2.18E-08	1.15E-08	6.20E-09	3.41E-09	1.09E-09	3.71E-10	1.33E-10	5.01E-11	1.25E-11	3.35E-12
6.00	1.75E-08	8.31E-09	4.06E-09	2.04E-09	1.05E-09	5.49E-10	1.60E-10	4.98E-11	1.64E-11	5.69E-12	1.26E-12	3.01E-13
7.00	3.96E-09	1.79E-09	8.38E-10	4.02E-10	1.96E-10	9.73E-11	2.66E-11	7.65E-12	2.33E-12	7.50E-13	1.49E-13	3.22E-14
8.00	9.57E-10	4.16E-10	1.87E-10	8.60E-11	4.06E-11	1.96E-11	4.88E-12	1.30E-12	3.70E-13	1.11E-13	2.00E-14	3.93E-15
9.00	2.44E-10	1.02E-10	4.42E-11	1.96E-11	8.95E-12	4.17E-12	9.67E-13	2.41E-13	6.43E-14	1.81E-14	2.97E-15	5.35E-16
10.00	6.52E-11	2.64E-11	1.10E-11	4.73E-12	2.08E-12	9.41E-13	2.05E-13	4.80E-14	1.20E-14	3.19E-15	4.80E-16	7.98E-17
12.00	5.13E-12	1.96E-12	7.69E-13	3.11E-13	1.29E-13	5.51E-14	1.07E-14	2.23E-15	5.02E-16	1.20E-16	1.54E-17	2.21E-18
14.00	4.47E-13	1.62E-13	6.05E-14	2.33E-14	9.19E-15	3.72E-15	6.51E-16	1.24E-16	2.52E-17	5.47E-18	6.13E-19	7.67E-20
16.00	4.19E-14	1.46E-14	5.21E-15	1.92E-15	7.24E-16	2.80E-16	4.49E-17	7.80E-18	1.46E-18	2.90E-19	2.87E-20	3.18E-21
18.00	4.17E-15	1.39E-15	4.94E-16	1.70E-16	6.17E-17	2.29E-17	3.40E-18	5.45E-19	9.42E-20	1.74E-20	1.53E-21	1.52E-22
20.00	4.33E-16	1.40E-16	4.66E-17	1.59E-17	5.59E-18	2.01E-18	2.77E-19	4.14E-20	6.67E-21	1.15E-21	9.17E-23	8.17E-24
22.00	4.66E-17	1.46E-17	4.73E-18	1.57E-18	5.33E-19	1.86E-19	2.40E-20	3.37E-21	5.08E-22	8.19E-23	5.94E-24	4.83E-25
24.00	5.15E-18	1.58E-18	4.97E-19	1.60E-19	5.30E-20	1.79E-20	2.19E-21	2.90E-22	4.12E-23	6.26E-24	4.14E-25	3.09E-26
25.00	1.73E-18	5.24E-19	1.63E-19	5.19E-20	1.60E-20	5.66E-21	6.73E-22	8.66E-23	1.20E-23	1.77E-24	1.12E-25	9.04E-27
26.00	5.84E-19	1.75E-19	5.37E-20	1.69E-20	5.40E-21	1.80E-21	2.09E-22	2.61E-23	3.52E-24	5.06E-25	3.09E-26	2.13E-27
28.00	6.74E-20	1.99E-20	5.95E-21	1.83E-21	5.78E-22	1.86E-22	2.06E-23	2.45E-24	3.14E-25	4.30E-26	2.43E-27	1.55E-28
30.00	7.91E-21	2.28E-21	6.73E-22	2.03E-22	6.27E-23	1.98E-23	2.09E-24	2.39E-25	2.92E-26	3.81E-27	2.01E-28	1.19E-29
32.00	9.41E-22	2.67E-22	7.74E-23	2.29E-23	6.95E-24	2.15E-24	2.18E-25	2.39E-26	2.80E-27	3.50E-28	1.72E-29	9.59E-31
34.00	1.13E-22	3.16E-23	9.03E-24	2.63E-24	7.85E-25	2.38E-25	2.33E-26	2.46E-27	2.77E-28	3.32E-29	1.54E-30	9.03E-32
35.00	3.95E-23	1.09E-23	3.10E-24	8.97E-25	2.65E-25	7.99E-25	7.68E-27	7.94E-28	8.78E-29	1.03E-29	4.65E-31	2.34E-32
36.00	1.35E-23	3.79E-24	1.07E-24	3.07E-25	8.99E-26	2.69E-26	2.54E-27	2.58E-28	2.80E-29	3.24E-30	1.42E-31	6.37E-33
38.00	1.69E-24	4.60E-25	1.28E-25	3.62E-26	1.04E-26	3.08E-27	2.82E-28	2.77E-29	2.90E-30	3.24E-31	1.34E-32	6.25E-34
40.00	2.09E-25	5.62E-26	1.54E-26	4.31E-27	1.23E-27	3.57E-28	3.18E-29	3.02E-30	3.07E-31	3.31E-32	1.30E-33	5.76E-35

Table 2. Calculated shield thicknesses for high energy proton synchrotrons.

Accelerator	Energy (GeV)	Beam loss (p/sec)	Radius (m)	L (GeV per cm·sec)	D (mrem/h)	L/D	Magnet thickness (g/cm^2)	Total shield thickness including magnet (g/cm^2) Gilbert et al.	This study
CPS	25.5	2×10^{11}	100	1.8×10^{7}	0.8[a]	2.3×10^{7}[b]	400	1085[c]	1085[c]
CPS	25.5	10^{12}	100	9.0×10^{7}	0.8	1.1×10^{8}[b]	400	1240	1240
CPS	25.5	10^{13}	100	9.0×10^{8}	0.8	1.1×10^{9}[b]	400	1455	1470
LRL design study	200.	2×10^{12}	693	9.2×10^{8}	1.25	7.4×10^{8}	280	1440	1430
	200.	2×10^{12}	693	9.2×10^{8}	0.25	3.7×10^{9}	280	1600	1590
CERN design study	300.	6×10^{12}	1200	2.4×10^{9}	0.8	3.0×10^{9}	300	1585	1570

a. Experimental value.
b. Effective value due to beam clipper.
c. Normalized to the same value.

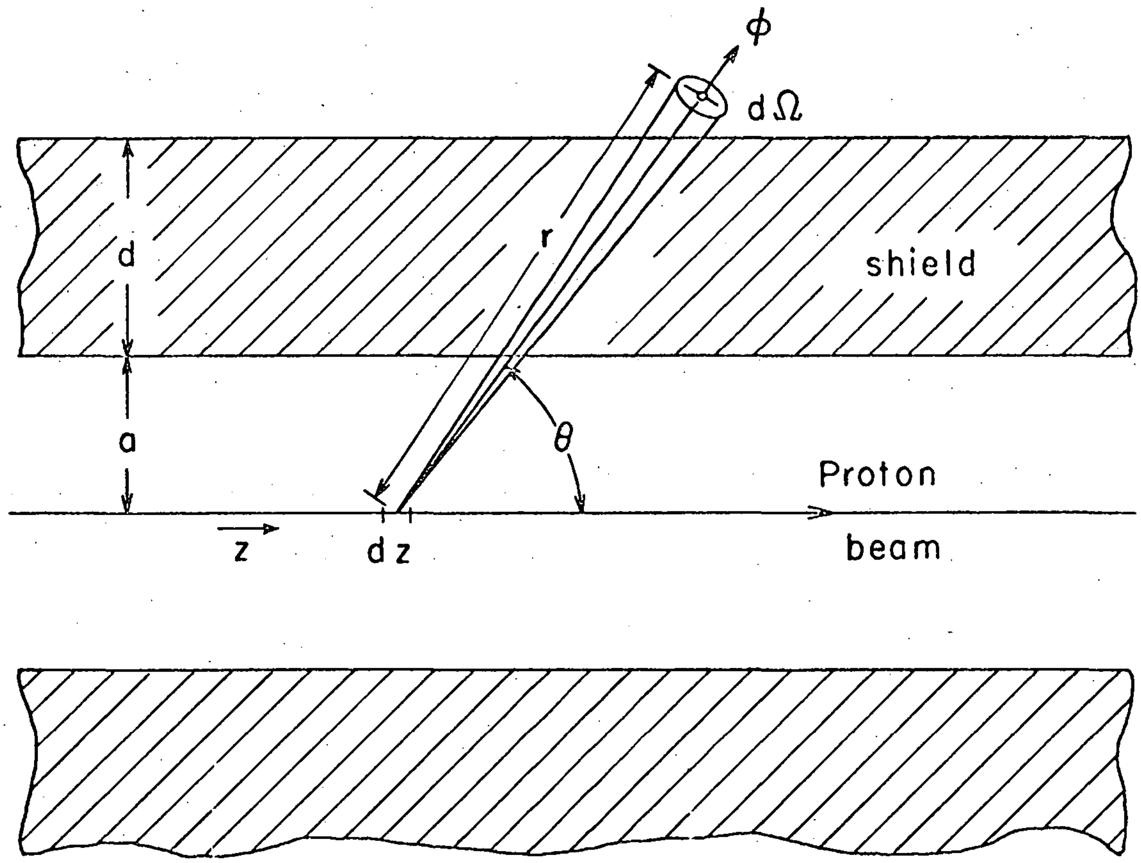

XBL694-2303

Fig. 1. Two-dimensional representation of the accelerator shielding geometry.

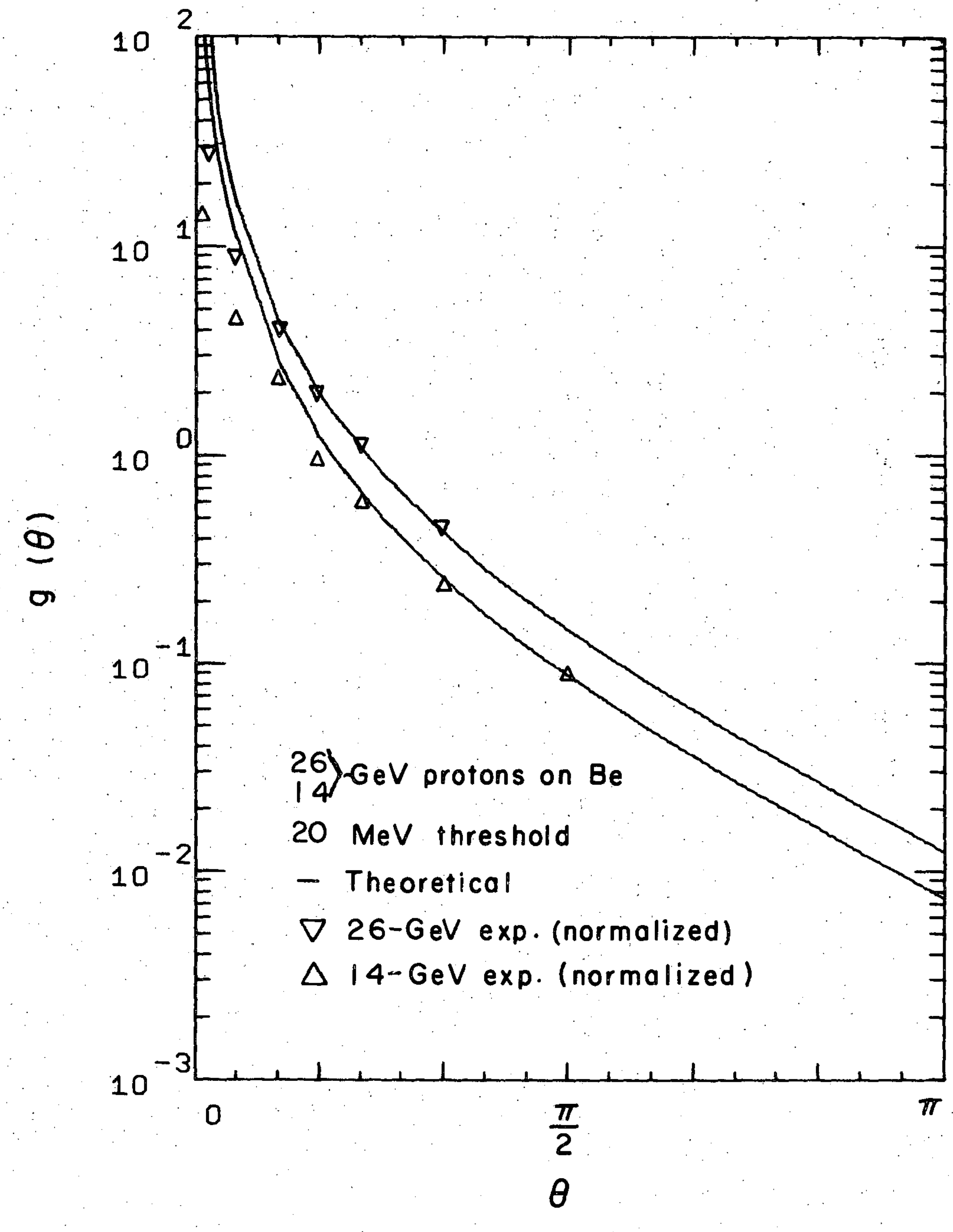

XBL694-2311

Fig. 2. The angular distribution of neutrons above 20 MeV energy produced by 26- and 14-GeV proton beam incident on a thin target, as measured by Gilbert et al., and calculated from Ranft formula.

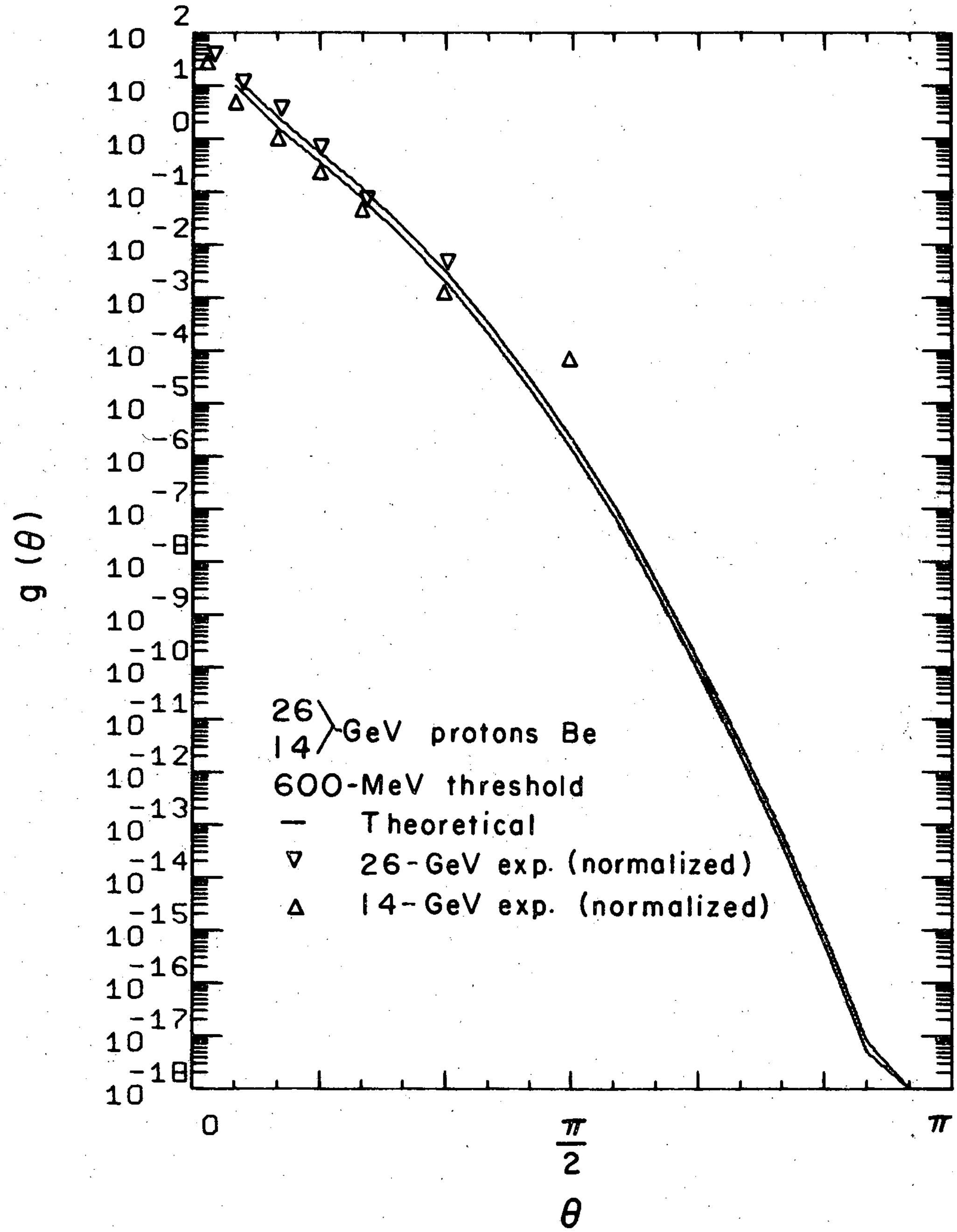

Fig. 3. The angular distribution of neutrons above 600 MeV energy produced by 26- and 14-GeV proton beam incident on thin target as measured by Gilbert et al., and calculated from Ranft formula.

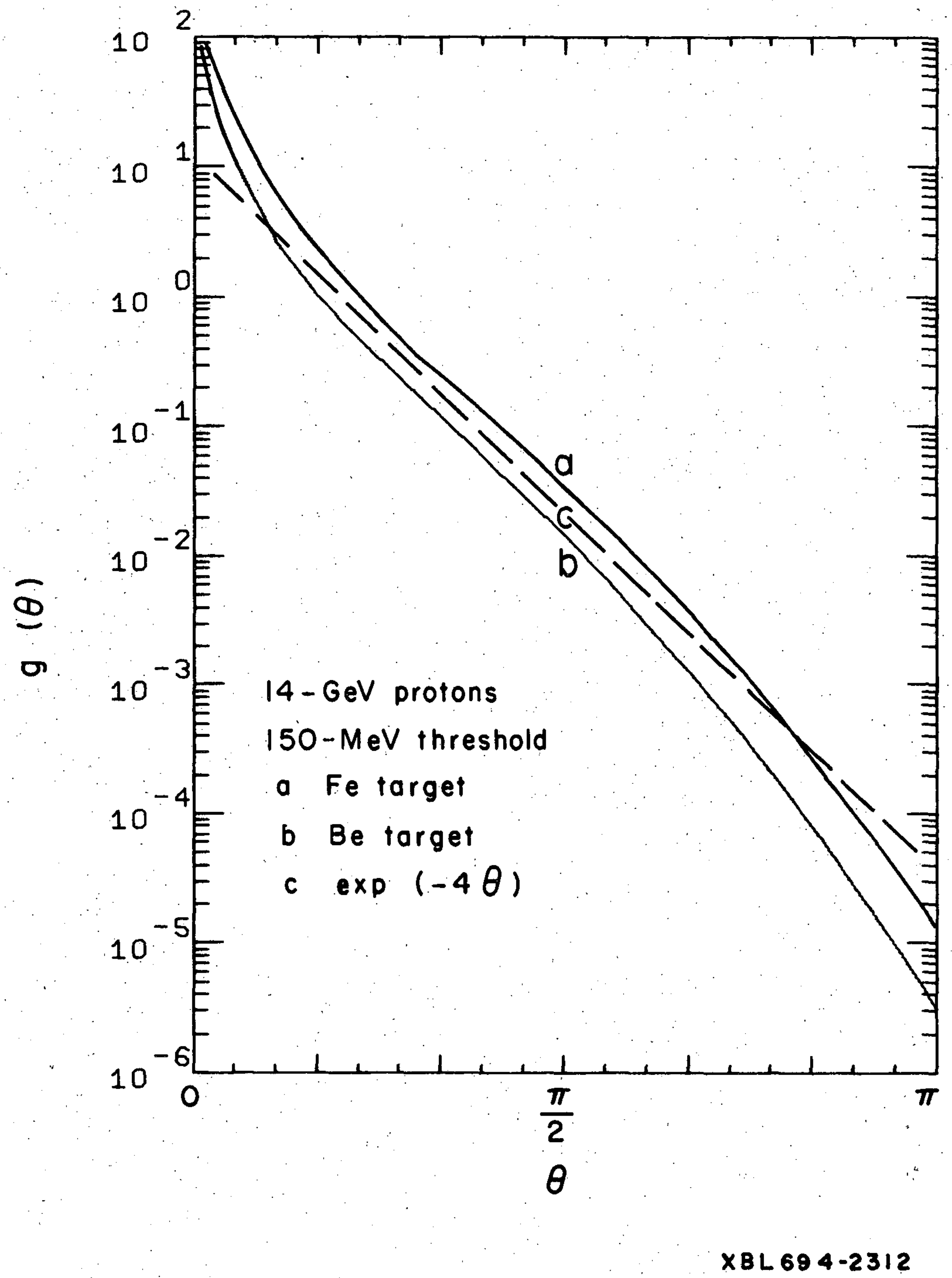

Fig. 4. The angular distribution of neutrons above 150 MeV energy produced by 14-GeV protons incident on thin Fe and Be targets as calculated from Ranft formula.

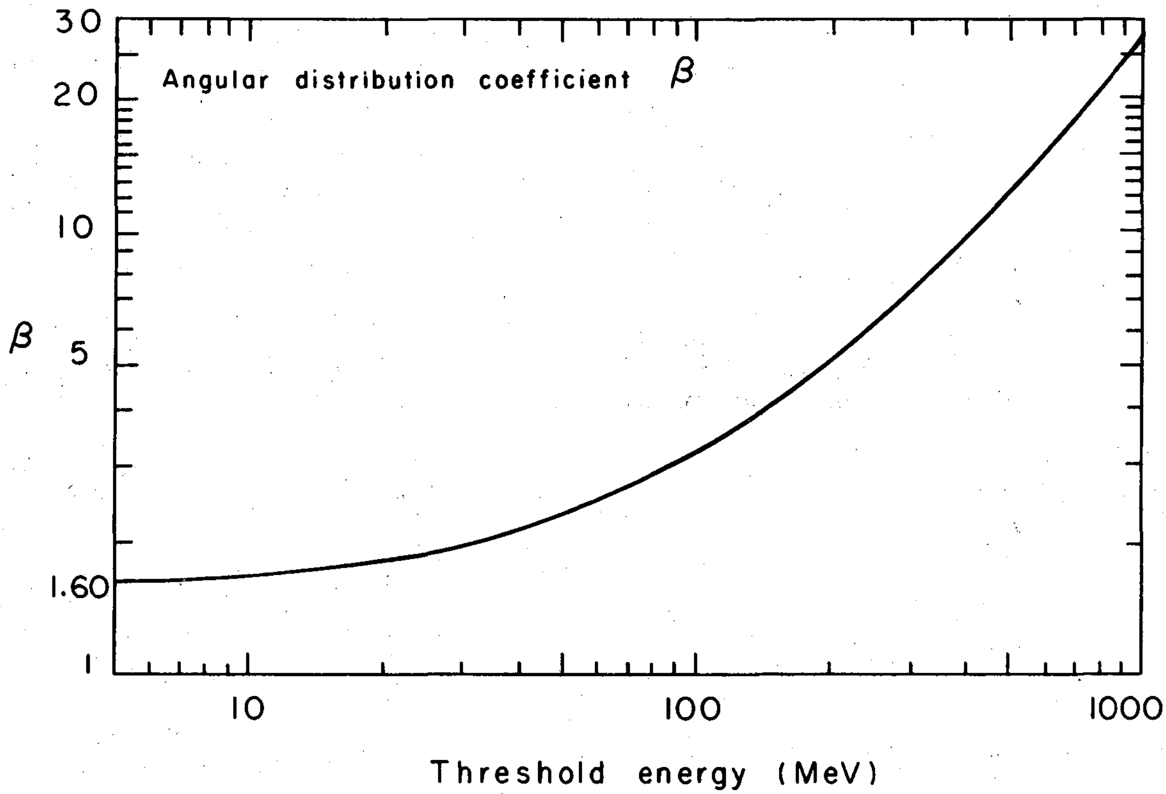

XBL694-2304

Fig. 5. The coefficient β in the angular distribution expression $g(\theta) = \alpha \exp(-\beta\theta)$ as calculated from Ranft formula for different threshold energies.

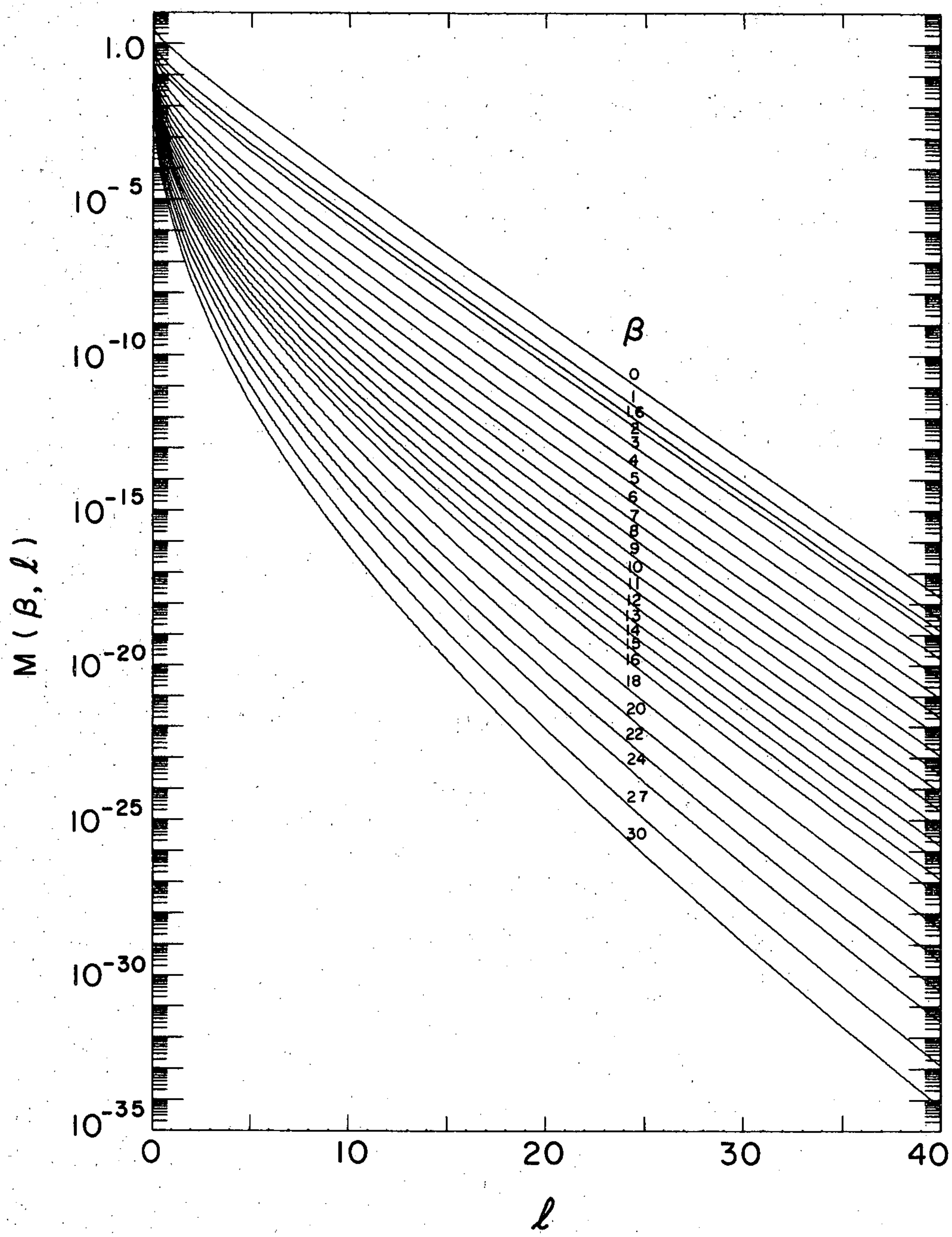

Fig. 6. Plot of Moyer Integrals for wide range of β and ℓ.

XBL694-2313

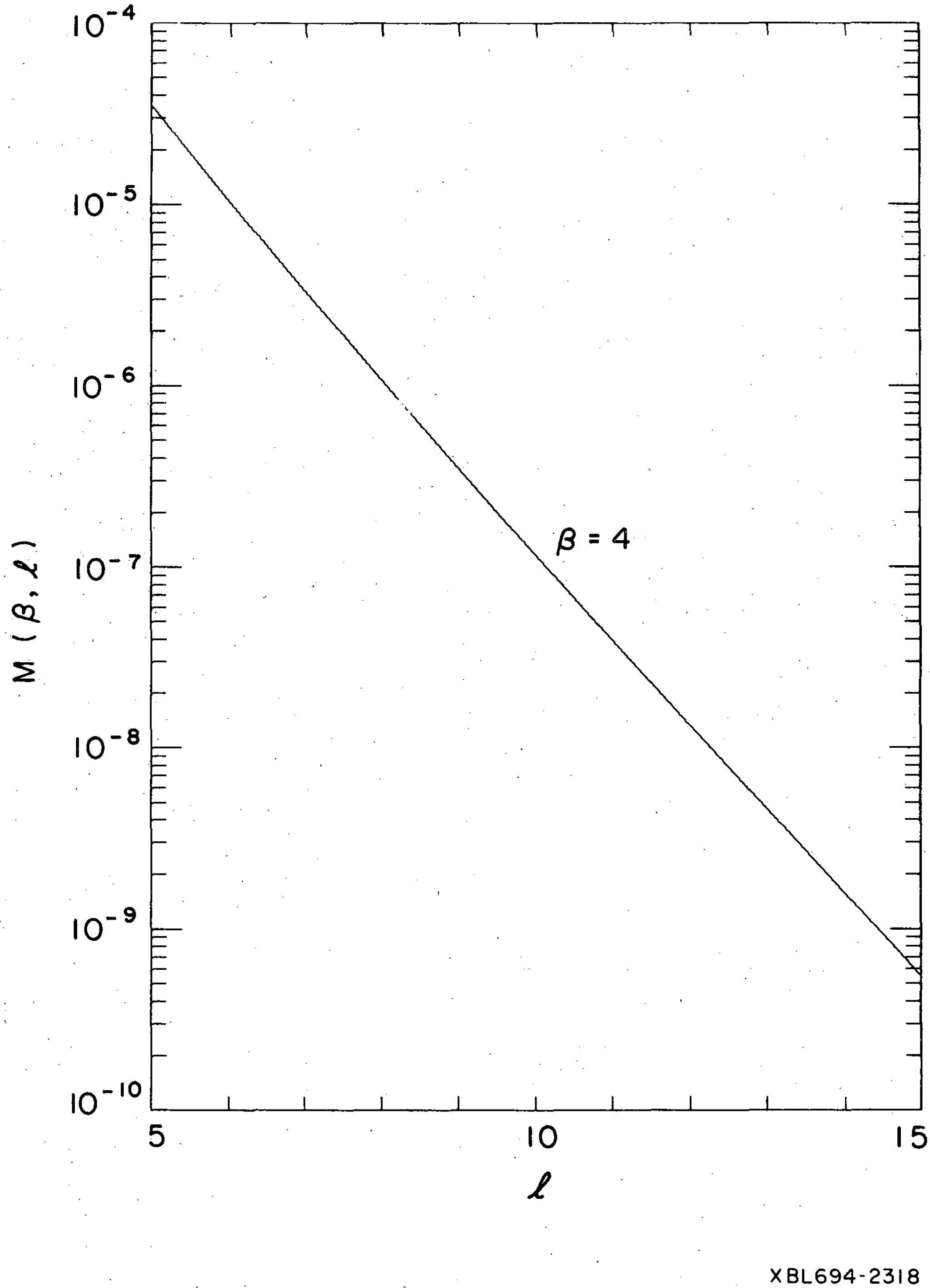

Fig. 7. Plot of Moyer Integrals for $\beta = 4$ corresponding to 150 MeV threshold energy, and a limited range of ℓ.

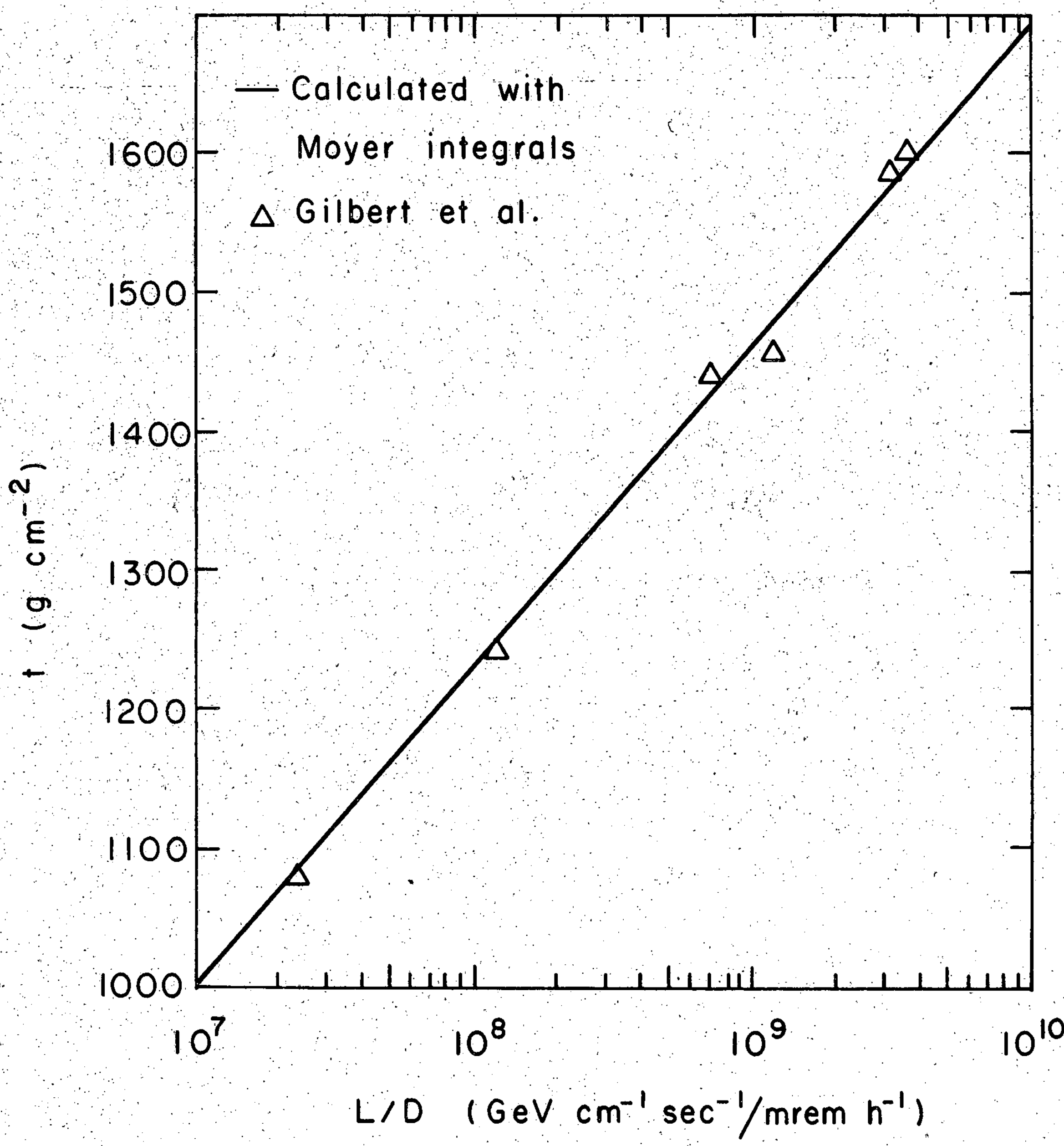

XBL 694-2305

Fig. 8. The total shield thickness obtained with the Moyer Integrals for different ratios of beam loss to dose rate, showing comparison to values by Gilbert et al., as listed in table 2.

TECHNICAL INFORMATION DIVISION
LAWRENCE RADIATION LABORATORY
UNIVERSITY OF CALIFORNIA
BERKELEY, CALIFORNIA 94720